Controlling Fluoride#Forming Reactions for Improved Rate Capability in Lithium#Perfluorinated Gas Conversion Batteries

Citation: Gao, Haining et al. "Controlling Fluoride#Forming Reactions for Improved Rate Capability in Lithium#Perfluorinated Gas Conversion Batteries." Advanced Energy Materials, 9, 21 (April 2019): 1900393 © 2019 The Author(s)

As Published: 10.1002/AENM.201900393

Publisher: Wiley

Persistent URL: https://hdl.handle.net/1721.1/127778

Version: Author's final manuscript: final author's manuscript post peer review, without publisher's formatting or copy editing

Controlling Fluoride-Forming Reactions for Improved Rate Capability in Lithium-Perfluorinated Gas Conversion Batteries

*Haining Gao, Yuanda Li, Rui Guo and Betar M. Gallant**

Y. Li, R. Guo, Prof. B. M. Gallant
Department of Mechanical Engineering, Massachusetts Institute of Technology, 77 Massachusetts Avenue, Cambridge, Massachusetts 02139, United States
E-mail: bgallant@mit.edu

H. Gao
Department of Materials Science and Engineering, Massachusetts Institute of Technology, 77 Massachusetts Avenue, Cambridge, Massachusetts 02139, United States

Keywords: lithium-gas battery, gas conversion, lithium fluoride, anion receptor, rate capability

Nonaqueous metal-gas batteries based on halogenated reactants exhibit strong potential for future high-energy electrochemical systems. The lithium-sulfur hexafluoride (Li-SF_6) primary battery, which utilizes a safe, noncombustible, energy-dense gas as cathode, demonstrates attractive eight-electron transfer reduction during discharge and high attainable capacities (> 3000 mAh/g_{carbon}) at voltages above 2.2 V_{Li}. However, improved rate capability is needed for practical applications. Here, we report two viable strategies to achieve this by targeting the solubility of the passivating discharge product, lithium fluoride (LiF). Operating at moderately elevated temperatures, e.g. 50 °C, in DMSO dramatically improves LiF solubility and promotes sparser and larger LiF nuclei on gas diffusion layer (GDL) electrodes, leading to capacity improvements of ~10x at 120 μA cm^{-2}. More aggressive chemical modification of the electrolyte by including a tris(pentafluorophenyl)borane (TPFPB) anion receptor further promotes LiF solubilization; capacity increased even at room temperature by a factor of 25 at 120 μA cm^{-2}, with attainable capacities up to 3 mAh cm^{-2}. This work shows that bulk fluoride-forming conversion reactions can be strongly manipulated by tuning the electrolyte environment to be solvating towards F^-, and that significantly improved rates can be achieved, leading a step closer to application.

1. Introduction

Continued demand for high-energy-density electrochemical power systems has drawn increasing attention to conversion-based systems,[1] especially nonaqueous Li-gas batteries, which have theoretical energy densities substantially higher (>5x) than Li-ion batteries.[2] While the majority of attention has focused on the Li-oxygen (Li-O_2) system due to its attractive energy density (3450 Wh $kg_{theoretical}^{-1}$, based on the weight of Li and O_2), improving rate capability,[3] and an earlier hope that it might be made rechargeable with continued development, significant challenges persist.[4] Among these are impermissibly high overpotentials required on charge (> 1 V), even when catalysts are employed, and pervasive side reactions, which together limit the electrochemical and chemical reversibility of the battery.

In light of these challenges, researchers have pursued two paths. The first of these has been to investigate alternatives to the Li anode for use with O_2 cathodes, for example sodium (Na)[5] and potassium (K)[6], due to the improved reversibility of their formed alkali oxides on charge.[7] However, replacing Li with Na or K substantially lowers the cell energy density, a main attraction of the O_2-based system in the first place. An alternative approach has focused instead on development of different types of gas cathodes that are inspired by the Li-O_2 system, yet are suited for a broader set of applications. Examples include oxide gases such as SO_2, which is currently a primary battery chemistry but exhibits potential to be made rechargeable;[8] CO_2-based batteries that attempt to extract end-of-life value from CO_2 while sequestering it in an electrochemical device;[9] or fluoride gases such as sulfur hexafluoride (SF_6) or nitrogen trifluoride (NF_3) for use in primary batteries, the latter of which have been developed recently in our group.[10] Although such systems may not be suited *a priori* for reversible energy storage, exploring new chemistries provides significant opportunity to develop new classes of high-capacity, high-energy conversion reactions, and to uncover new electrochemical mechanisms that may be employed in future primary

or rechargeable batteries. In particular, perfluorinated gases, which are energy-dense, are typically stable or even inert in the reactant state,[11] and therefore offer additional advantages in terms of safety and storage compared to O_2, e.g. for military or space applications. Thus, "beyond Li-O_2" batteries provide flexibility to the metal-gas family while filling in gaps in energy-power metrics for broader applications.

Developing higher-energy electrochemical systems can be achieved by identifying high-potential or high-capacity reactions, or ideally both. Identifying new reaction with high capacities is non-trivial, given the inherent limitations in transition-metal redox (typically 1 e^-/transition metal for conventional intercalation cathodes), or in oxygen molecular redox (typically a one- or two-electron transfer reaction at room temperature).[12] Although a 4-electron reaction has very recently been achieved in Li-O_2 system in molten salt-based electrolytes, higher temperatures (150 °C) were required.[13] In contrast, halogenated molecules, with a highly-oxidized central atoms such as carbon (e.g. CF_4), nitrogen (NF_3) or sulfur (SF_6), open up new opportunities in the design of lower-temperature multi-electron transfer reactions. High (n_{e^-}>2) electron transfer numbers can be theoretically proposed, and scale proportionally with the number of fluoride ligands. The discharge reactions result in ligand abstraction and reaction with alkali metal ions, with concurrent reduction of the central atom to a neutral or reduced state. Recently, we demonstrated that the full reductions of two perfluorinated gases, NF_3 (to N_2(g) and LiF, nitrogen oxidation state change of 3) and SF_6 (to Li_2S/S and LiF, sulfur oxidation state change of 6 to 8), can be realized in Li-based cells, and illuminated their discharge reaction mechanisms on carbon electrodes at room temperature.[10] While high capacities were achieved (e.g., ~3600 mAh g_C^{-1} at 75 mA g_C^{-1} for SF_6), roughly comparable in scale to the Li-O_2 system on similar Vulcan carbon cathode materials (~3000 mAh g_C^{-1} at ~100 mA g_C^{-1}),[14] the discharge potentials were several hundred millivolts lower than typical Li-O_2 cell voltages, (~ 2.3 V vs. Li/Li^+ compared to ~2.7 V vs. Li/Li^+, respectively), and cells

exhibited poor rate capability. Thus, the future attractiveness of such systems depends on the ability to improve the attainable energy density and increase the performance at higher currents. In this work, we demonstrate that such improvements are possible.

One of the major challenges currently limiting the attainable energy density in metal-gas systems in general is the eventual passivation of the electrode surface due to buildup of insulating solids. In the Li-O_2 system, premature "sudden death" is mainly caused by coverage of active surfaces by Li_2O_2, an electronic insulator.[15] Therefore, to enable higher capacities, a central strategy has been to increase the solubility of the reduction intermediate, the superoxide radical anion O_2^-. This can be achieved intrinsically, either by utilizing electrolyte solvents with high Guttman donor number (DN)[16] and/or acceptor number (AN);[17] or through incorporation of chemically-specific additives such as redox mediators,[18] solution aggregation promotors such as molecular sieves,[19] or electrode functionalities that promote solution-phase Li_2O_2 growth.[20] Notably, such strategies are not unique to metal-gas systems, and have been employed as well in solid-solid conversion reactions, for instance to mediate the passivating effects of bulk LiF formation in Li-CF_x batteries. Strategies, including optimizing electrolyte solvents (for example using dimethyl sulfoxide (DMSO)),[21] and incorporating electrolyte additives (such as anion receptors),[22] has been applied to improve the Li-CF_x battery performance significantly by promoting fluoride solvation.

In Li-fluorinated gas systems, a similar "sudden death" phenomenon occurs, caused by the buildup and eventual passivation of LiF. Whereas both SF_6 and NF_3 reduction reactions were found to exhibit high overpotentials (> 1 V) on discharge due to the difficulty of the first electron-coupled activation and fluoride expulsion step,[10] the capacity was also dramatically curtailed at only moderate current densities (~100 mA g_C^{-1}), which represented the more severe contribution to poor rate capability. In this work, we focus on strategies to improve the rate performance by addressing

the latter point, using the SF_6 conversion reaction as a model fluoride-forming system. The nominal cell discharge reactions are

$$\text{Anode: } 8\text{Li} \rightarrow 8e^- + 8\text{Li}^+$$

$$\text{Cathode: } \text{SF}_6 + 8e^- + 8\text{Li}^+ \rightarrow 6\text{LiF} + \text{Li}_2\text{S}$$

$$\text{Cell reaction: } \text{SF}_6 + 8\text{Li} \rightarrow 6\text{LiF} + \text{Li}_2\text{S}\ ,\ \text{E}^\circ = 3.69\ \text{V vs. Li/Li}^+$$

with a theoretical energy density of 3922 Wh kg^{-1}. In practice, a mix of Li_2S, S, and reduced polysulfides were found after discharge, reflecting impartial reduction of some sulfur species prior to their dissolution and/or electrochemical isolation in the electrode.[10a] Regardless, LiF was by far the majority product, formed at a 6-fold higher rate than sulfur-derived products, and thus is the species that we target for capacity improvements in the present study.

Herein, we report three strategies to improve the rate capability of Li-SF_6 batteries by modifying the electrolyte solvent and reaction conditions to promote LiF solubility. First, we explored the discharge performance of SF_6 in Li cells in a wide range of commonly-utilized battery solvents to identify trends that support high capacity. We find that DMSO with both a high DN and acceptor number (AN), showed good LiF solubility as well as stability against polysulfide species, in contrast to carbonates and ether-based solvents, both of which yield substantially lower capacities. Utilizing room-temperature DMSO cells as a benchmark, we investigated the Li-SF_6 discharge behavior at elevated temperatures of 50 °C to better understand the sensitivity of kinetics and/or solubility to thermal activation. Finally, we investigate the prospect of incorporating a commonly-utilized anion receptor, tris(pentafluorophenyl)borane (TPFPB), to promote LiF solubilization at high discharge rates. With TPFPB, a more than 25-fold increase in capacity can be achieved at high currents of 120 μA cm^{-2}.

2. Results and Discussion

We hypothesized that, analogous to Li-O_2 systems, the electrolyte solvent might influence the solubility of SF_6 reduction intermediates (lower fluorides of SF_6, F^-, or LiF) and thus the growth of LiF crystallites during discharge. To investigate this, the discharge behavior of Li-SF_6 cells was first examined in six typical solvents: DMSO, N,N-dimethylacetamide (DMA), diethylene glycol dimethyl ether (diglyme), tetraethylene glycol dimethyl ether (TEGDME), ethylene carbonate/diethyl carbonate (EC/DEC), and propylene carbonate (PC). Lithium perchlorate ($LiClO_4$) was chosen as the salt to avoid a possible additional fluoride source. To avoid possible reaction between Li and electrolyte solvents, Li metal was stabilized in PC electrolyte before being used as the anode.[23] Trends were first examined on porous Vulcan carbon (VC, ~100 m^2 g^{-1})[24] electrodes, comparable to those used previously. As shown in **Figure 1**, the solvent had a strong effect on the discharge behavior. At 75 mA g_C^{-1}, the carbonates PC and EC/DEC exhibited limited capacities of 630 and 735 mAh g_C^{-1}, respectively, and had low voltage plateaus of ~1.9 V vs. Li/Li^+ (**Figure 1a**). These relatively low capacities can be attributed in part to the known reactivity of polysulfides with carbonate-based electrolytes, which likely forms passivating decomposition products on the electrode.[25] Meanwhile, ether-based electrolytes yielded significantly higher capacities (~1345 mAh g_C^{-1} for diglyme and ~1170 mAh g_C^{-1} for TEGDME), and the discharge voltages were also found to be approximately 100 mV higher, at ~2.0 – 2.1 V vs. Li/Li^+. A more dramatic improvement in both capacity and voltage was observed with both DMA (2445 mAh g_C^{-1} at ~2.40 V vs. Li/Li^+) and DMSO (4250 mAh g_C^{-1} at ~2.45 V vs. Li/Li^+). This trend was also well-reproduced on gas diffusion layer (GDL) electrodes discharged at comparable low rates of 5 μA cm^{-2} (**Figure 1b**; all corresponding argon backgrounds exhibited negligible capacity, **Figure S1**). Although GDL has relatively low surface area (~1 m^2 g^{-1})[5a] and is not optimized for practical batteries, in this study, GDL is valuable for standardizing the electrode porosity and surface area from cell to cell and providing suitable visual contrast to examine the discharge product

morphology (discussed later in the text). Thus, GDL electrodes are utilized (unless otherwise noted) in the remainder of the study.

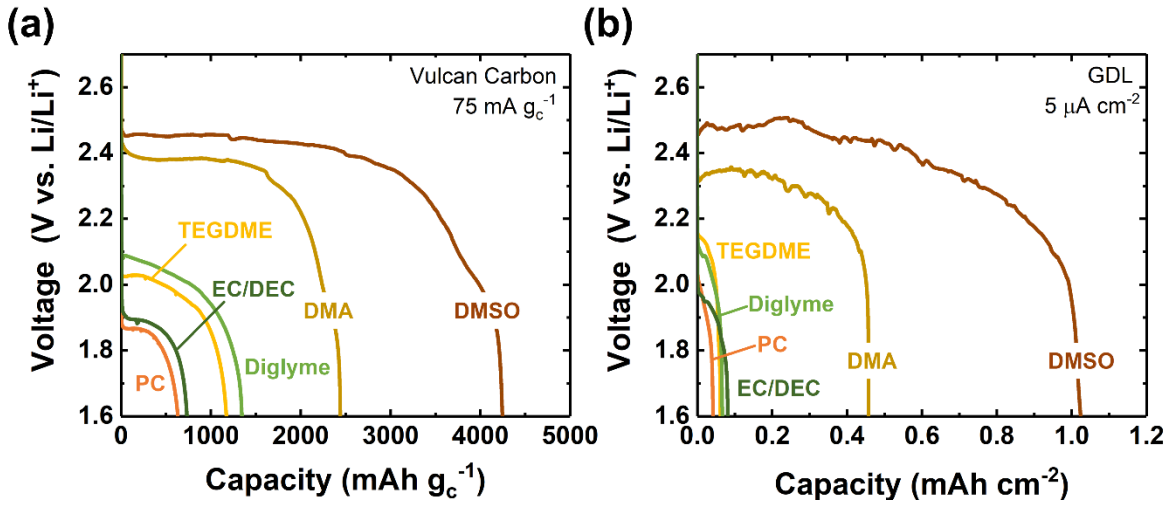

Figure 1. Galvanostatic discharge profiles of Li-SF_6 cells in various solvents, as indicated, with a lower cutoff voltage of 1.6 V vs Li/Li^+ on **(a)** Vulcan carbon or **(b)** gas diffusion layer (GDL) cathodes. Electrolytes contained 0.1 M $LiClO_4$ (TEGDME, DMSO, EC/DEC, PC and DMA) or 0.07 M $LiClO_4$ (diglyme). For GDL electrodes, capacity and current density are normalized to the GDL geometric area.

We considered three parameters to explain the performance trends of the solvents studied herein: LiF solubility; solvent acceptor number (AN); and donor number (DN). However, as LiF is only slightly soluble in water (1.33 g L^{-1} at 291 K),[26] and is considered virtually insoluble in organic solvents,[27] the solubility in organic electrolytes has not been consistently reported (although it is known to be higher in DMSO, 0.37 g L^{-1},[28] compared to e.g. PC or DEC; see **Table S1**). Meanwhile, whereas LiF solubility is descriptive of the intrinsic ability of a solvent to stabilize both F^- and Li^+, donor and acceptor number reflect the individual strength of solvent interaction with Lewis acids (e.g. Li^+) or bases (e.g. F^-), respectively. Although the elemental electrochemical steps of SF_6 reduction are not currently known, SF_6 has been reported to decompose by rapid fluoride ion rejection[29] and our previous study of the perfluorinated gas analogue, NF_3, showed electron-coupled fluoride expulsion to be the likely conversion mechanism.[10b] Thus, it is probable that "lone" metastable F^- may be generated during discharge, with finite lifetimes in the electrolyte

before complexation with Li^+ and subsequent precipitation. Indeed, a strong correlation between DN and total achievable capacity was observed: ethers, having relatively low DN (16 for TEGDME and 18 for diglyme),[30] showed lower SF_6 discharge capacity, whereas DMSO (DN = 29.8) and DMA (DN = 27.8)[30b] delivered the highest. For solvents with comparable DN, higher AN (DMA = 13.6, DMSO = 19.3)[30b] also supported higher capacity. Such trends are similar to those observed in Li-O_2 batteries, where high DN solvents such as DMSO promote solution-phase growth of Li_2O_2 by strongly solvating Li^+ and limiting its rate of reaction with superoxide.[31] Thus, we conclude that similar effects govern the growth of LiF and lead to higher capacities in the SF_6 system. Higher DN solvents have also been reported to increase polysulfide solubility in Li-sulfur batteries, which may aid here as a secondary effect against S/Li_2S passivation.[32] As DN and AN are more widely reported and experimentally accessible than LiF bulk solubility, these metrics may aide in future prediction of additional solvents that support high-capacity SF_6 discharge.

Comparisons of discharged electrodes were made to investigate whether the solvent modulated the discharge product morphology. **Figure 2a** shows scanning electron microscopy (SEM) images of cathodes discharged to a limited capacity of 0.05 mAh cm^{-2}, which is low enough to be reached in all solvents, at 5 μA cm^{-2}. X-ray diffraction (XRD) performed on electrodes discharged in all five solvents (**Figure S2**) confirmed that LiF was the only detectable crystalline product, and therefore, in the following, we interpret the morphologies as being predominantly reflective of LiF. From the images, it is evident that the cathodes for solvents that exhibit low discharge capacity, i.e. rapid electrode passivation (EC/DEC, PC, diglyme, and TEGDME), generally showed uniform LiF coverage consisting of many small LiF particles. In contrast, the cathode in high DN solvents (DMSO and DMA) exhibited sparser particles with more available carbon surface area, consistent with the ability to continue discharge to much higher capacities. The variation of average particle size in different electrolytes is quantified in **Figure 2b**. A general

trend of increasing particle size with achievable discharge capacity is observed, which reflects the ability to form more microscopically three-dimensional and thus less passivating particles in DMA and DMSO. DMSO, which gave the highest capacity, showed significantly larger average particle size (~90 nm) compared to all others (< 40 nm). Overall, it is evident that the LiF nuclei at low capacity vary dramatically in different solvents, and their nanoscale morphologies underlie the ability to undergo continued discharge to high capacities. Given the apparently unique ability of DMSO to promote high capacities, we select it as the solvent for continued study.

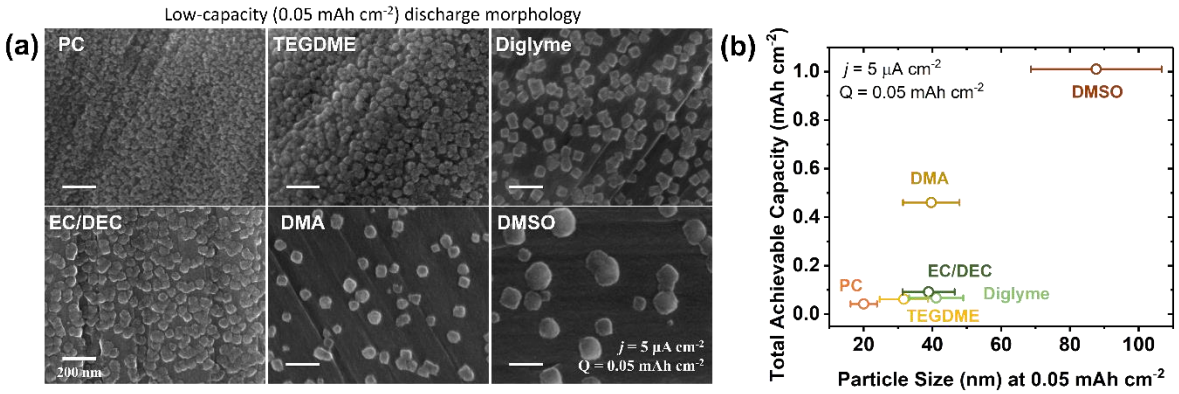

Figure 2. (a) SEM images of cathodes discharged to a limited capacity of 0.05 mAh at 5 μA cm^{-2} in PC, EC/DEC, TEGDME, DMA, diglyme, and DMSO electrolyte. **(b)** Total achievable discharge capacity (from Figure 1b) as a function of average particle size observed by SEM in different solvents at limited capacity (0.05 mAh cm^{-2}). Average and error bars reflect statistics over at least 20 particles.

The rate capability at full capacity was next investigated in DMSO on GDL over a range of current densities, as shown in **Figure 3a**. Between 5 and 120 μA cm^{-2}, the discharge capacity decreased by almost an order of magnitude, from approximately 1.0 to 0.1 mAh cm^{-2}, and was accompanied by a decrease in discharge potential of around 0.4 V, from 2.5 to 2.1 V vs. Li/Li^+. The high sensitivity of voltage to discharge rate is comparable with other metal-gas batteries discharged on non-catalyzed carbon electrodes.[33] To confirm that the capacity was limited by LiF passivation and not transport in DMSO, Rotating Disk Electrode (RDE) measurements were conducted in SF_6-saturated DMSO electrolyte using glassy carbon (GC) as working electrode

(**Figure S3**). Even at a rotation speed of 1600 rpm, limiting current behavior could not be reached under cyclic voltammetry conditions at 100 mV s^{-1}, and a comparable total reduction capacity of 2.1 μAh cm^{-2} was obtained in all cases regardless of rotation rate, due to rapid passivation once the onset of SF_6 reduction began. Negligible anodic current was detected on the forward scan, indicating the non-rechargeability of the Li-SF_6 system, in agreement with that observed in our previous study.[10a] Furthermore, significant impedance increase detected during discharge (**Figure S4a**) also provided evidence for electrode passivation. We therefore concluded that the reactions under given electrochemical conditions (galvanostatic or cyclic voltammetry) are always limited by LiF passivation, even though higher capacities are achievable in DMSO compared to other solvents.

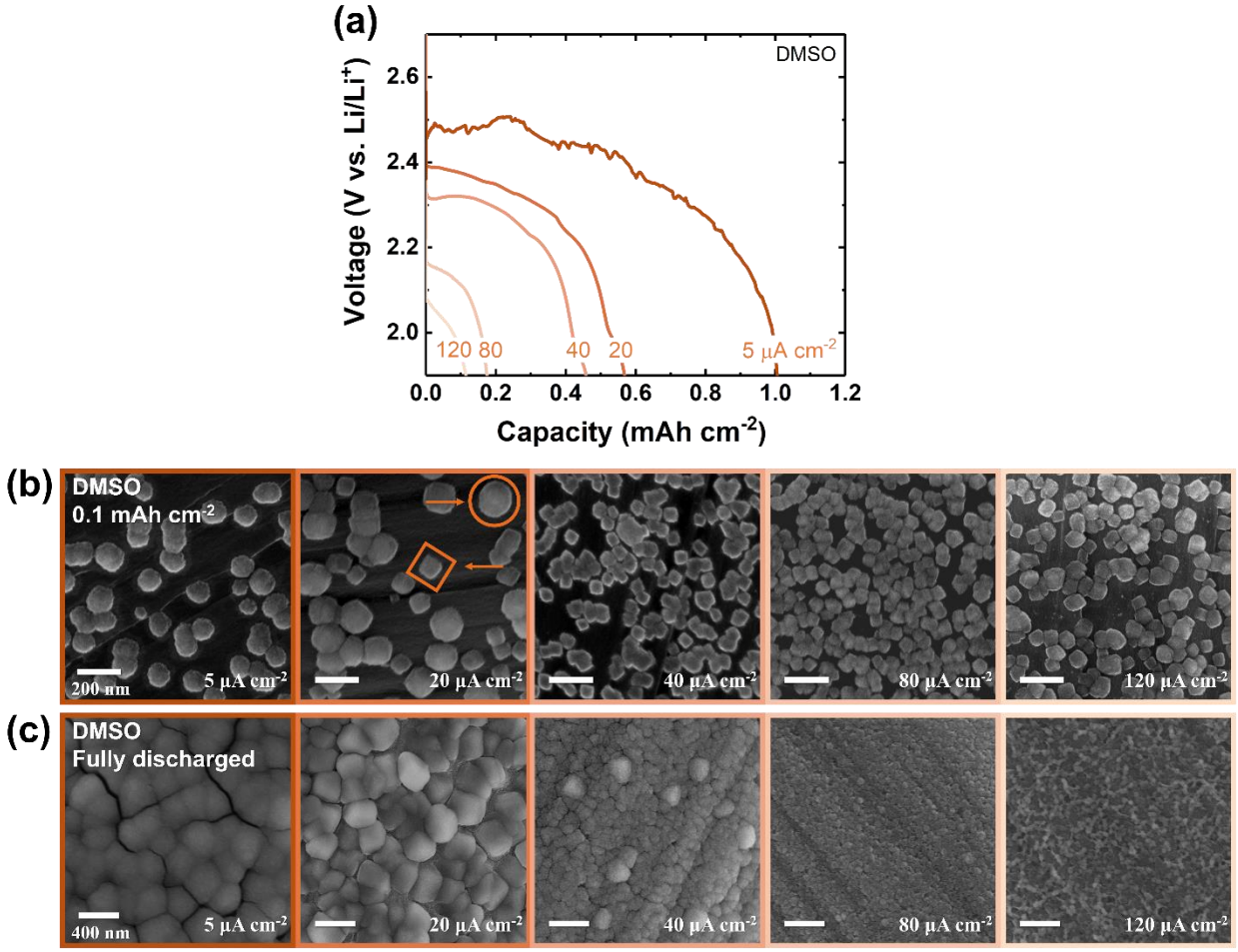

Figure 3. (a) Galvanostatic discharge profiles of Li-SF_6 cells in DMSO electrolyte at current densities of 5, 20, 40, 80 and 120 μA cm^{-2}. SEM image of cathodes discharged to **(b)** 0.1 mAh cm^{-2} and **(c)** fully discharged at different current densities (as indicated) in DMSO.

The structure of the LiF particles, in addition to being solvent-dependent, was also highly rate-dependent. Limited-capacity morphologies at 0.1 mAh cm^{-2} are shown in **Figure 3b** for current densities up to 120 μA cm^{-2}. At low rates of 5 μA cm^{-2}, sparser and rounder nuclei (~110 nm) were observed at 0.1 mAh cm^{-2}; these gradually became more cube-shaped and smaller (~60 nm) at increasing current densities. At an intermediate current density of 20 μA cm^{-2}, a mix of spheres and cubes was seen, indicating a transition between the two morphologies. These distinct morphologies were retained up to full discharge capacities (**Figure 3c**). We note that similar results were observed in DMA, i.e., the surface was fully passivated by larger, although less spherical, LiF particles at

full capacity (**Figure S5**). However, the LiF particles were smaller in DMA than in DMSO, consistent with a larger population of active nuclei and more rapid passivation in DMA.

Given the central role of the spherical LiF deposits in supporting higher capacities, we investigated whether thermal effects can promote enhanced formation of this desired morphology. Discharge performance of Li-SF_6 cells was evaluated at a moderately higher temperature of 50 °C, as shown in **Figure 4a**, for current densities ranging from 40 to 500 μA cm^{-2}. We confirmed that the higher temperature did not modify the background currents under argon, as indicated in **Figure S6**. The corresponding rate capability of Li-SF_6 cells with DMSO electrolyte at room temperature (RT) and 50 °C are compared in **Figure 4b.** At a relatively low current density of 40 μA cm^{-2}, the discharge capacity at 50 °C reached 1.8 mAh cm^{-2}, more than four times higher than the capacity observed at room temperature (~0.4 mAh cm^{-2}). Meanwhile, at a higher current density of 120 μA cm^{-2}, whereas severe performance loss was already observed under room temperature conditions (discharge voltage < 2.1 V vs. Li/Li^+ and only ~ 0.1 mAh cm^{-2}), at 50 °C the cell could retain a capacity above 1.0 mAh cm^{-2} and a voltage of 2.3 V. Severe performance loss was only observed at rates higher than 300 μA cm^{-2}. Note that a trend of increasing temperature yielding higher capacity and potential was also previously observed in Li-O_2 and Li-NF_3 batteries.[10b, 34] In the Li-SF_6 system, the improvement at higher temperature is related both to increased solubility of LiF and, to likely lesser effect, lithium sulfide or polysulfide, as indicated by the modified morphologies; but also to improved kinetics, as reflected in the higher average discharge potentials. These higher voltages achieved at elevated temperature help to support the selective activation of fewer nucleation sites while promoting their growth to substantially larger sizes (~350 nm, compared to ~50 nm at room temperature; **Figure 4c** and **Figure S7**). A temperature increase from 25 °C to 45 °C was found in a separate study to increase LiF solubility by nearly a factor of two, from 0.37

g L^{-1} to 0.60 g L^{-1}, in DMSO,[28] in agreement with the electrochemical and morphological results observed here.

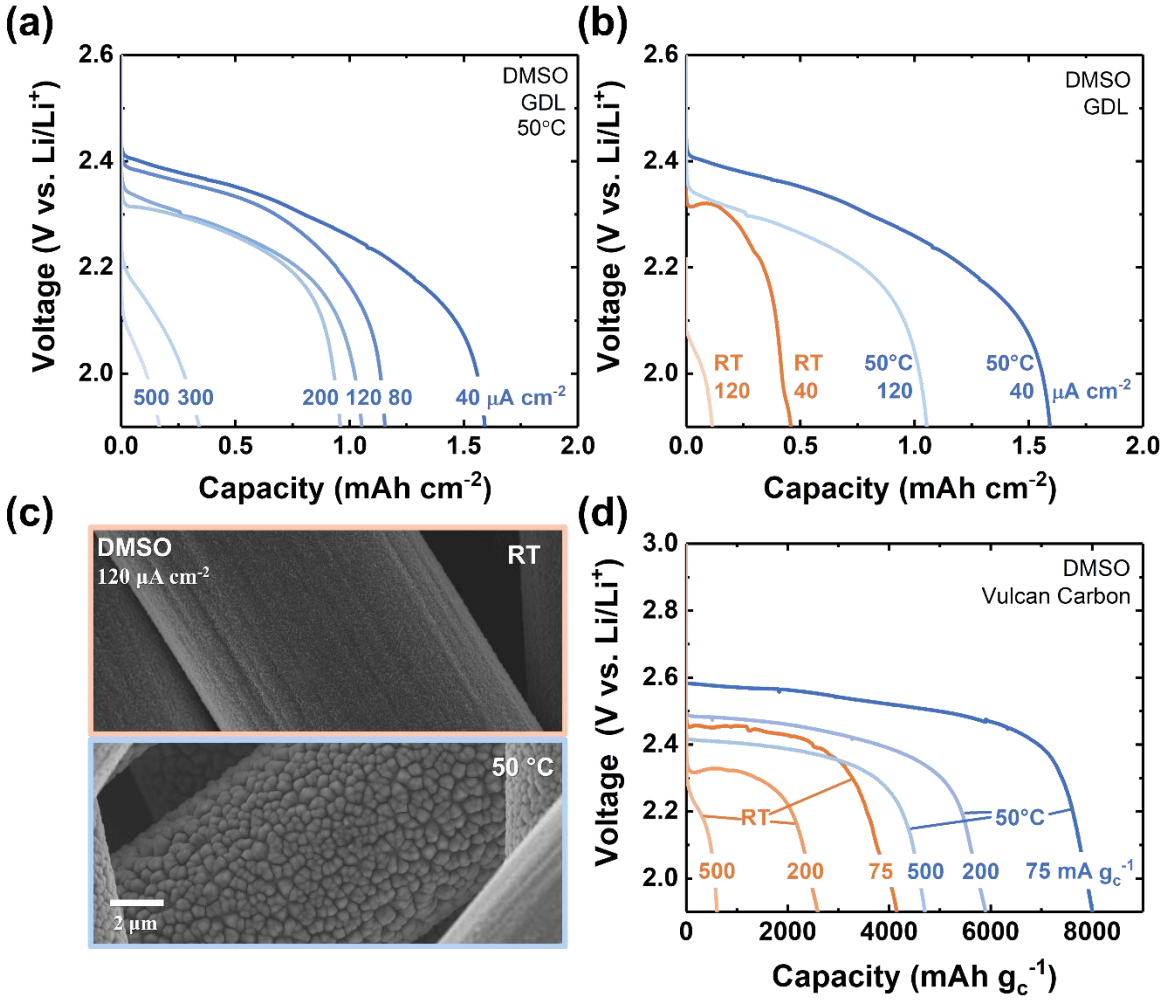

Figure 4. Li-SF_6 cells at 50 °C. **(a)** Galvanostatic discharge profile of Li-SF_6 cells in 0.1 M $LiClO_4$/DMSO electrolyte with GDL electrodes at current densities from 40 to 500 µA cm^{-2} (lower voltage cutoff of 1.9 V vs Li/Li^+). **(b)** Comparasion of discharge profiles at 50 °C and room temperature (RT) at current densities of 40 and 120 µA cm^{-2}. **(c)** SEM image of a GDL cathode fully discharged at 120 µA cm^{-2} at 50 °C (lower) and RT (upper). **(d)** Discharge profile of Li-SF_6 cells in DMSO electrolyte with Vulcan carbon electrodes at 75, 200 and 500 mA g_C^{-1} at RT and 50 °C.

Figure 4d shows that these substantial performance gains, obtained on GDL, could also be translated to the more practical Vulcan carbon electrodes. A nearly two-fold increase in capacity (~ 8000 mAh g_C^{-1} at 50 °C), as well as a ~0.1 V increase in discharge potential (from less than 2.5 V to ~ 2.6 V vs. Li/Li^+) was observed at moderate currents of 75 mA g_C^{-1}. Moreover, capacities

remained greater than ~4500 mAh g_C^{-1} at 500 mA g_C^{-1}. Overall, the results indicate that moderate temperature increases can dramatically alter the LiF nucleation and growth process, resulting in sizeable gains in performance and enabling high-rate performance. However, LiF passivation is still ultimately the limiting factor, which is supported by the SEM images at full discharge along with electrochemical impedance measurements, which show significantly larger resistances as depth of discharge increased (**Figure S4b**). Thus, we next investigated an additional strategy to further improve the capacity at room temperature based on chemically-specific promotion of LiF solubility.

Tris(pentafluorophenyl)borane (TPFPB), with a molecular structure as shown in **Figure 5a**,[35] is among the family of borate-based anion receptors that contain electron-deficient Lewis acid centers effective for binding F^- and promoting LiF solubilization.[36] Thus, it has been used previously as an additive in Li-ion batteries at low concentrations (typically < 0.1 M) to increase the solubility of LiF formed from parasitic decomposition of fluorine-containing electrolyte salts,[37] or to promote silicon[38] or graphite[39] anode stability. More recently, TPFPB has been used in Li-O_2 batteries to catalyze superoxide disproportionation.[40] However, to the best of our knowledge, TPFPB has not been used previously in large concentrations as a participant in a bulk fluoride-forming reaction. Thus, we began by exploring the feasibility of using TPFPB at the high fluoride-forming rates in Li-SF_6 systems. To do so, passivation was initially exacerbated by using the low-surface area, "planar" GC electrode in the RDE configuration, where passivation effects can be readily detected as early as the first scan, as discussed previously.

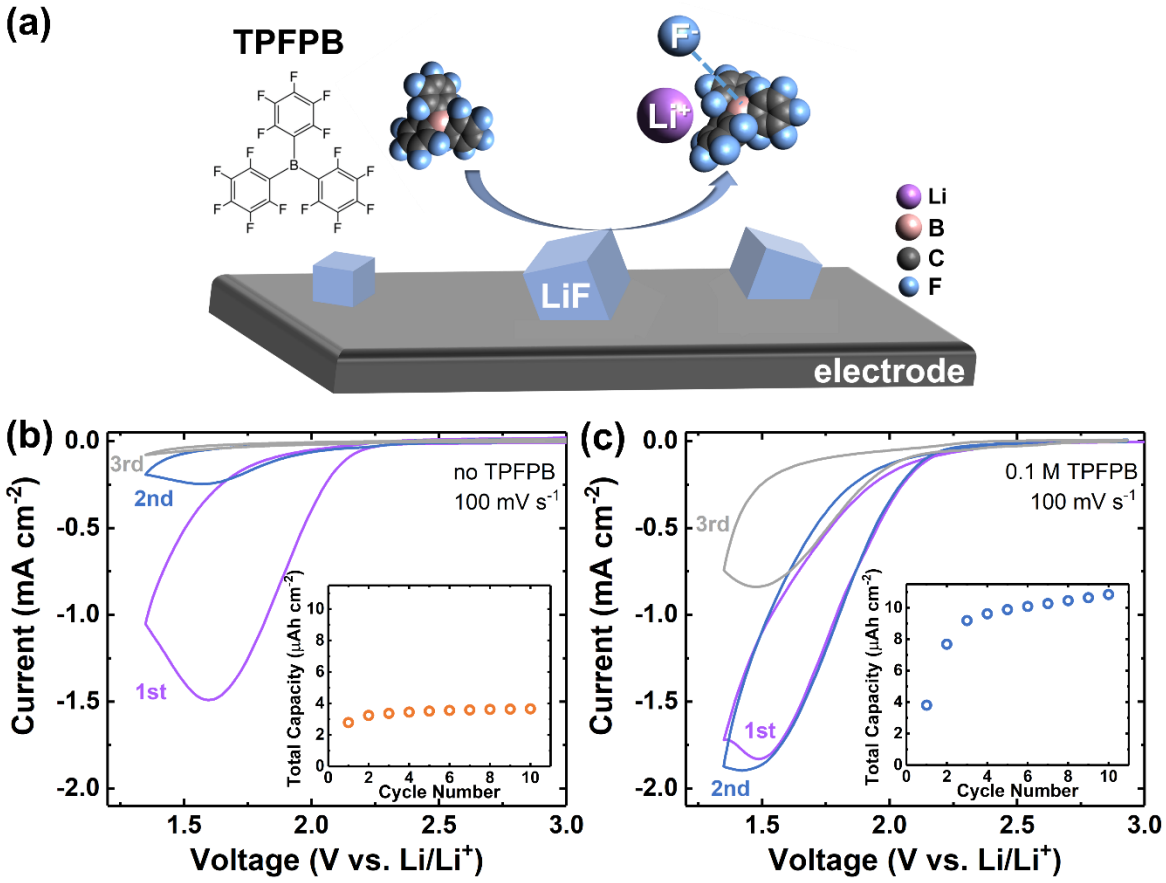

Figure 5. **(a)** Schematic depicting the anion receptor, TPFPB, which promotes LiF solvation by forming a complex with F^- anions. Cyclic voltammetry traces and the total capacity (inset) of SF_6-saturated electrolyte containing **(b)** 0.1 M $LiClO_4$/DMSO, and **(c)** 0.1 M TPFPB with 0.1 M $LiClO_4$/DMSO at a scan rate of 100 mV s^{-1}.

Figure 5b,c shows the first three CV scans in DMSO electrolyte at a fast scan rate of 100 mV s^{-1}, without and with TPFPB additive at a concentration of 0.1 M. Note that when TPFPB was used, the lower voltage cutoff was set as 1.35 V vs. Li/Li^+ (instead of 1.0 V vs. Li/Li^+, as in Figure S3) to avoid parasitic reduction of TPFPB, which was found to be significant below ~1.3 V vs. Li/Li^+ (**Figure S8**). Without TPFPB (**Figure 5b**), the carbon electrode was nearly passivated on the second scan, and the integrated reduction capacity (figure inset) reached a rapid plateau after the 2nd cycle, at < 4 μAh cm^{-2}. With TPFPB present, however, the peak current reached on the first scan was modestly higher (~1.9 mA cm^{-2} vs. ~1.5 mA cm^{-2}) and nearly comparable currents were retained on the second scan. Continued cycling was still possible after that, albeit with passivation

becoming more predominant. Consequently, the integrated reduction capacity (figure inset, **Figure 5c**) increased rapidly and reached a higher steady-state value greater than 10 μAh cm^{-2}. Note that these gains were achieved at a relatively high scan rate of 100 mV s^{-1}, and are expected to be even more pronounced at lower rates. Thus, having established the feasibility of using TPFPB to dissolve passivation-scale amounts of LiF during SF_6 reduction, we further investigated its effect under more practical galvanostatic conditions in Swagelok cells with GDL electrodes.

The capacity of Li-SF_6 cells was found to depend sensitively on the concentration of TPFPB. Cells were characterized at a typical current density of 40 μA cm^{-2}, which correponds to an intermediate F^- generation rate (assuming 8 e^-/SF_6) of 4.7×10^{-10} mol s^{-1} or 3.1 μM s^{-1} (based on the electrolyte volume of 150 μL). Prior to discharge experiments, we confirmed that the Li, pre-stabilized by soaking in PC electrolyte, was chemically stable against TPFPB by performing ^{19}F NMR analysis of electrolytes in contact with Li over long soaking times (six days), which indicated negligible reactivity and no loss of TPFPB (**Figure S9** and **Table S2**). As shown in **Figure 6a**, the attainable capacity scaled monotonically with TPFPB concentration up to 3.0 mAh cm^{-2} at 400 mM, indicating the strong contribution from TPFPB in solubilizing LiF (discharge under argon headspace with TPFPB yielded negligible capacity, **Figure S10**). Meanwhile, higher TPFPB concentrations yielded slightly lower discharge potentials (by ~50 mV) at 400 mM, due to increased viscosity at higher concentrations. The capacity improvement, defined as the difference with and without TPFPB at each current density, was calculated and compared to the theoretical capacity gain assuming that each TPFPB molecule dissolves only one molecule of LiF, as might be expected if the TPFPB becomes saturated after reaction (see SI for calculation details). As shown in **Figure 6b**, the actual capacity gain is significantly larger than this theoretical value at all currents. This greater-than-predicted capacity improvement suggests that some amount of F^- turnover occurs, or in other words, that each molecule of TPFPB dissolves more than one LiF, perhaps by facilitating

its deposition in more energy-favorable sites *via* a solution-precipitation route that frees TPFPB for solubilization of additional LiF. Assuming this mechanism, the turnover rate of TPFPB at concentrations of 50, 200 and 400 mM could be calculated as 5.1, 2.2 and 1.6, respectively. This indicates that the gains in capacity decreased with increasing TPFPB concentration, especially at higher concentrations of 200 and 400 mM, where viscosity was significant and may have impeded precipitation and turnover of TPFPB. We note that higher viscosity was also reflected in impedance measurements, which indicated an order-of-magnitude increase in charge-transfer resistance when 400 mM TPFPB was added to the electrolyte (**Figure S4c**, compared with Figure S4a). We note that the major crystalline discharge product in the discharged cathodes spanning the range of additive concentrations used was confirmed to still be LiF, as indicated by XRD (**Figure 6c**). Consistent with the above picture, the LiF formed in the presence of TPFPB was substantially more three-dimensional and porous compared to the TPFPB-free case, as revealed in SEM images (**Figure 6d**). At higher concentrations of 400 mM, the particles were still three-dimensional in appearance, yet had smaller diameters than at 50 or 200 mM. We again attribute this to the high viscosity at 400 mM, which may limit transport of bulky TPFPB from the electrode surface, resulting in more rapid precipitation and smaller LiF particle growth. Interestingly, the inclusion of TPFPB appeared to alter the discharge state of sulfur, which was predominantly present in reduced form in previous work.[10a] Through quantitative ^{19}F NMR analysis, the total amount of fluoride formed can be compared with that expected, based on either a 6- or 8-electron transfer reaction (**Figure S11a**). Whereas both room-temperature and 50 °C discharge in DMSO quantitatively produced LiF consistent with a predominantly 8-electron transfer reaction, slightly higher amounts of LiF were present with TPFPB with respect to the number of electrons transferred, corresponding to a ~6-electron process. This could be confirmed by X-ray photoelectron spectroscopy measurements post-discharge with TPFPB (**Figure S11b**), in which S_8 was the major

S-containins species present in the electrode, in contrast to our previous work.[10a] The detailed elementary reaction steps require future efforts to elucidate in full and a future study is planned dedicated to the influence of electrolyte on sulfur redox processes near the end of discharge.

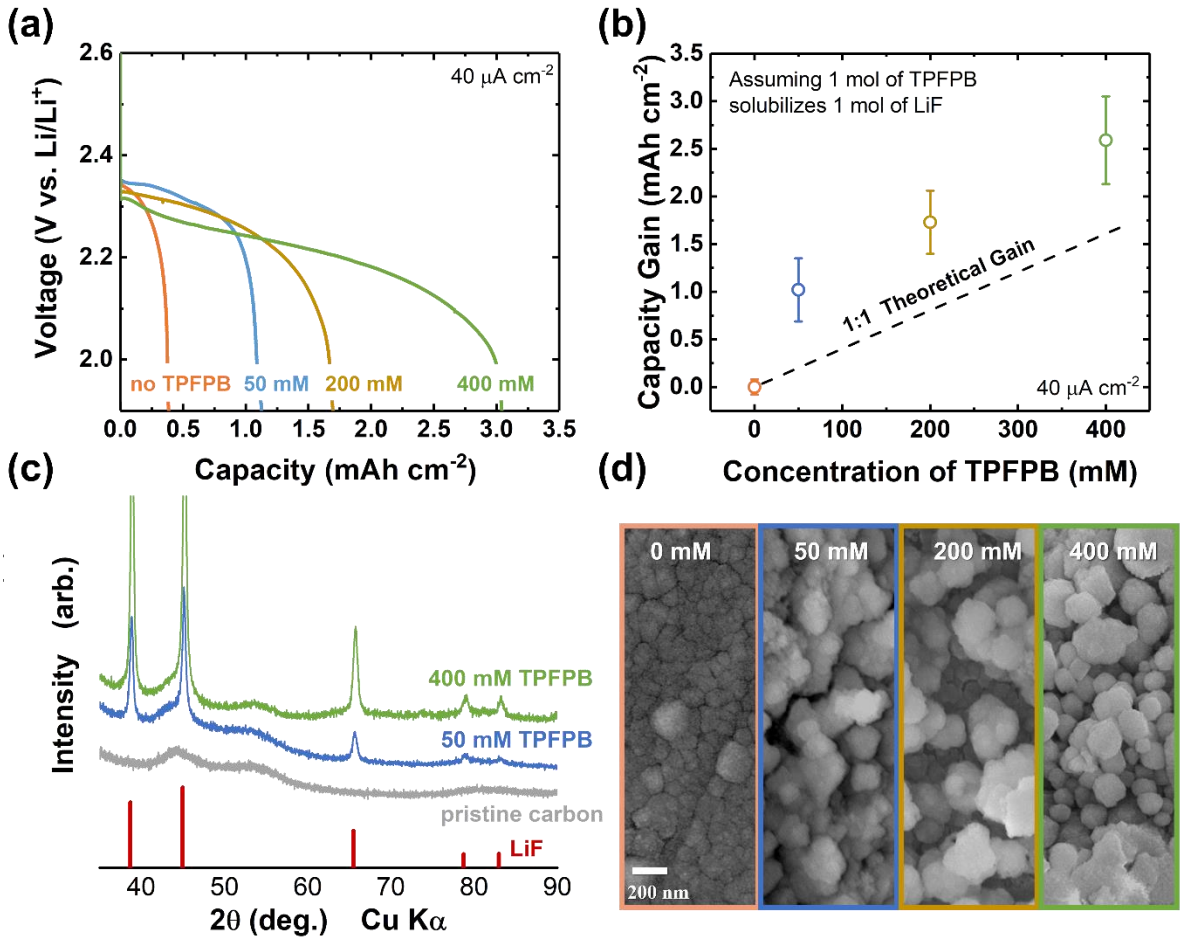

Figure 6. (a) Galvanostatic discharge profiles of Li-SF_6 cells at 40 μA cm^{-2}. The electrolyte was 0.1 M $LiClO_4$/DMSO containing 0, 50, 200 or 400 mM TPFPB. **(b)** Theoretical (dashed line) and observed (circles) average capacity gain at the corresponding TPFPB concentration. The averages and error bars represent statistics from more than three samples for each condition. **(c)** XRD pattern of the pristine GDL and cathodes fully discharged in electrolyte containing 50 and 400 mM TPFPB at 40 μA cm^{-2}. **(d)** SEM images of cathodes fully discharged at 40 μA cm^{-2} in DMSO electrolyte with different TPFPB concentrations (as indicated).

The rate capability improvements attainable with 400 mM TPFPB from 40 – 120 μA cm^{-2} are summarized and compared with the other two systems in this work. The individual rate capability profiles of cells with 400 and 200 mM TPFPB are given in **Figure S12**. As shown in

Figure 7, at moderate rates (40 μA cm^{-2}), higher temperature increased the discharge capacity by approximately five-fold, from 0.4 to 1.8 mAh cm^{-2}. Meanwhile, TPFPB increased the capacity by a factor of seven (to 2.8 mAh cm^{-2}). The capacity gains were even larger at higher currents. For example, at 120 μA cm^{-2}, the capacity increased by an order of magnitude by elevating the cell temperature to 50 °C, and by a factor of 25 when adding TPFPB. Although we did not explore combining these two effects (higher temperature and TPFPB), it is likely that even higher capacities could be obtained by capitalizing on both effects; however, special care will be needed to ensure TPFPB stability at higher temperatures. Overall, these results indicate that tailoring the LiF solubility presents a promising route to dramatically increase the energy density attainable at higher rates, a key limitation in our original study. We note that TPFPB is not necessarily an optimized choice among the many different choices of anion receptor available commercially,[41] and therefore, further gains in improvement may be achievable, particularly if less-bulky anion receptors can be identified to minimize viscosity increases at higher concentrations. Overall, these improvements open the door for further development of bulk solid-forming reactions for sustained power delivery in halogenated-molecular conversion reactions.

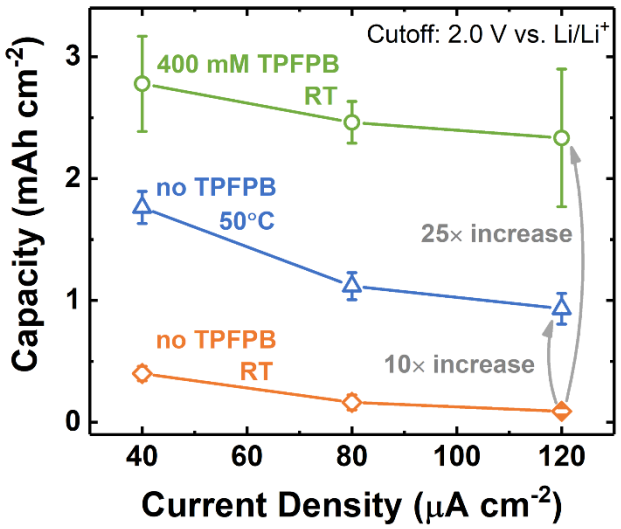

Figure 7. Comparison of rate capability of Li-SF_6 cells at 50 °C and RT with or without TPFPB additive, obtained on GDL electrodes in 0.1 M $LiClO_4$/DMSO electrolyte at a cutoff voltage of 2.0 V vs. Li/Li^+. The averages and error bars represent statistics from more than three samples for each condition.

3. Conclusions

We have reported viable strategies to dramatically improve the attainable capacity, and thus the energy density, in Li-SF_6 cells undergoing bulk fluoride-forming reactions. Both approaches explored herein target the intrinsically low solubility of LiF, either by operating at moderately elevated temperatures of 50 °C to improve solubility and favor sparser and larger LiF nuclei in the initial stages of growth; or through more aggressive chemical modification of the electrolyte to incorporate an anion receptor additive (TPFPB) that dissolves LiF. Both strategies can significantly increase the achievable capacity by a factor of 10 and 25 respectively, at a high current density of 120 μA cm^{-2}. Use of anion receptors, in particular, appears promising for applications where operating at higher temperature may not be an option. Combining this approach with future efforts to increase the discharge voltage, for instance by altering the electrode material to promote specific SF_6 adsorption and/or catalyze its reduction,[42] may lead to even closer realization of the high theoretical energy densities intrinsic to the Li-SF_6 system.

4. Experimental Section

Chemicals and Materials: All chemicals, electrodes and cell-making materials were thoroughly dried and stored in an argon-filled glovebox (H_2O content <1 ppm, O_2 content <1 ppm, MBRAUN). $LiClO_4$ (99.99% trace metals basis, Sigma-Aldrich) and TPFPB (>97%, Alfa Aesar) were dried for 24 hours at 70 °C and 90 °C, respectively, in a Buchi glass oven. Diglyme (99.5%, Sigma-Aldrich), TEGDME (99%, Sigma-Aldrich), PC (99.7%, Sigma-Aldrich), DMSO (> 99.9%, Sigma-Aldrich), EC (99%, Sigma-Aldrich), DEC (> 99.9%, Sigma-Aldrich) and DMA (99.8%, Sigma-Aldrich) were dried over fresh molecular sieves (Type 3 Å, Sigma-Aldrich) inside the glovebox at room temperature for 24 hours prior to use. The molecular sieves and Whatman filter paper (Grade QM-A, 2.2 μm pore size, 450 μm in thickness, Sigma Aldrich) were dried overnight at 120 °C under active vacuum in a glass oven (Buchi).

Carbon Cathode Preparation: The Vulcan carbon (VC) cathodes were fabricated in-house by uniformly coating sonicated inks composed of VC (XC-72, Cabot Corporation), isopropanol, and lithiated Nafion (LITHion dispersion, Ion Power, with a Nafion/VC weight ratio of 1:2) onto a sheet of Celgard separator (Celgard 2325, 25 μm thickness, MTI Corporation). The obtained VC-coated Celgard was dried at room temperature before being punched into circular disks (12 mm diameter), with a typical VC loading of 0.27 ± 0.08 mg_C cm^{-2} (error bar represents four measurements). The as-received gas diffusion layer (GDL, Freudenberg H23, FuelCellStore) was also punched into 12 mm diameter discs. The VC and GDL cathodes were subsequently dried under active vacuum in a glass oven (Buchi) overnight at 70 °C and 120 °C, respectively.

Galvanostatic Discharge: Two-electrode Swagelok-type Li-SF_6 cells were constructed in an argon glovebox, with VC or GDL as cathode and a 9 mm diameter disk of Li metal as anode (0.75 mm

thick, 99.9% metals basis, Alfa Aesar), which was prestabilized by soaking in 0.1 M $LiClO_4$ in PC for more than three days before use.[23] The separator (13 mm diameter glass fiber filter paper) was impregnated with 150 μL electrolyte solution. The $LiClO_4$ concentration in DMSO, TEGDME EC/DEC (50/50 v/v), PC and DMA electrolytes were 0.1 M, while the only exception was diglyme, where the concentration was 70 mM owing to a lower salt solubility limit. SF_6 gas (Airgas, 99.999% purity) was introduced into cells following their assembly by purging SF_6 into the cell headspace within the glovebox for approximately 3 min, pressurizing it to ~1.6 bar, and then sealing the cell for subsequent measurement outside the glovebox.

Li-SF_6 cells were rested at open circuit voltage (OCV) for 15 hours prior to testing. Typical open circuit voltage (OCV) values of assembled cells ranged from 2.7 – 3.3 V (vs. Li/Li^+). The subsequent galvanostatic discharge measurements were carried out (BioLogic VMP3 potentiostat or MPG2 workstation) at the specified current density with a voltage window ranging from open circuit to a lower cutoff voltage of 1.6 - 2.0 V vs Li/Li^+(as indicated). The lower cutoff voltage was varied in different measurements to avoid the decomposition of electrolyte, particularly when the anion receptor, TPFPB, was added. Results (current density and capacity) were normalized to the geometric area of GDL or the weight of VC used. For galvanostatic discharge at 50 °C, the cells were placed inside an incubator (Memmert GmbH + Co. KG). For cells using DMA electrolyte, due to its reactivity with Li, pre-oxidized $LiFePO_4$ (LFP) was used as anode. The LFP electrode (9 mm diameter, single-side coated on Al foil, MTI Corporation, 7.63 mg) was first charged at a current density of 0.2 C for 15 min in a Li-LFP Swagelok-type cell with 1 M $LiPF_6$ in EC/DEC electrolyte (v/v = 1/1, battery grade, Sigma-Aldrich). After pre-delithiation, the electrode was extracted from the cell and rinsed before used in LFP-SF_6 cells. The LFP-SF_6 cell voltage was converted to Li/Li^+ scale by adding the measured oxidation potential of LFP (3.44 V vs. Li/Li^+).

The capacity of LFP-SF_6 DMA cells was in all cases < 1 mAh, below the capacity remaining in the LFP electrodes (~1.23 mAh).

Rotating Disk Electrode (RDE) Measurements: Three-electrode electrochemical measurements were carried out in an argon-filled glovebox. All the electrodes and glass cells were purchased from Pine Research Instruments. The reference electrode was constructed by immersing a silver wire into a ceramic-fritted glass tube filled with 0.01 M $AgNO_3$ and 0.1 M $TBAClO_4$ in acetonitrile. For the counter electrode, a Pt wire was inserted in a fritted glass compartment that was filled with working electrolyte. A glassy carbon (GC) disk (0.196 cm^2) was used as working electrode. Prior to each measurement, the GC electrode was polished using de-ionized water-wetted polishing papers (Thorlabs) in a sequence of 5, 3, 1, and 0.3 μm until a mirror finish was obtained, followed by a rinsing step with de-ionized water, and was dried under active vacuum in a glass oven (Buchi) at 70 °C overnight. The electrode was transferred into glovebox directly without exposure to air.
To determine the potential of reference electrode versus Li/Li^+, a piece of Li foil was inserted into the electrolyte solution and its potential relative to Ag/Ag^+ was measured until stabilization. The obtained value were: 0 V_{Li} = -3.65 V vs. Ag/Ag^+ in 0.1 M $LiClO_4$ in DMSO; 0 V_{Li} = -3.64 V vs. Ag/Ag^+ in 0.1 M TPFPB / 0.1 M $LiClO_4$ in DMSO. After the Li/Li^+ potential was established, the working electrode was then immersed in the electrolyte and repeatedly cycled at 100 mV s^{-1} with a passive argon headspace between 3 V and 1 V (vs. Li/Li^+) until a stable capacitive background current was obtained. The GC electrode was then replaced with a freshly-polished electrode, and SF_6 was bubbled into the electrolyte for at least 5 min prior to cyclic voltammetry (CV) measurements. For rotating disk electrode measurements, the rotation rate of GC electrode was controlled by a Modulated Speed Rotator (Pine).

Scanning Electron Microscopy (SEM): After discharge, the Li- SF_6 cell was disassembled inside the glovebox and the cathode was extracted, rinsed with 1,2-dimethoxyethane and dried in the argon glovebox prior to SEM characterization. The sample, which was sealed in a glass vial in the glovebox, was then quickly transferred into the SEM chamber for the measurement to minimize exposure to ambient. All the SEM characterizations were conducted on a Zeiss Merlin High-resolution SEM operating at an accelerating voltage of 5 kV and beam current of 100 pA.

X-ray Diffraction (XRD): The pristine and rinsed discharged cathodes were all stored inside the glovebox. Prior to XRD measurements, the samples were sealed in an air-sensitive sample holder in the glovebox to minimize atmospheric contamination. XRD patterns were collected on a PANalytical X'Pert Pro multipurpose diffractometer with a copper anode (Cu Kα). All scans for cathode characterization were performed from $5° < 2\theta < 90°$ at a typical scan speed of $0.5° \text{ min}^{-1}$. Reference data for LiF: space group: $Fm\bar{3}m$, JCPDS: 00-004-0857.

Spectroscopic Measurements: ^{19}F Nuclear Magnetic Resonance (NMR) measurements were performed using a Bruker Advance Neo 400 MHz NMR spectrometer. Samples dissolved in deuterated solvents (D_2O (Sigma-Aldrich) or DMSO-d_6 (Sigma-Aldrich)) with 2,2,2-trifluoroethanol (TFE, Sigma-Aldrich) or trifluoroacetic acid (TFA, Sigma-Aldrich) as reference. Samples were then transferred into capped NMR tubes (Wilmad, 528-PP-7) or coaxial tubes (Wilmad, 517-complete) for NMR analysis. X-ray photoelectron spectroscopy (XPS) analysis was conducted on a PHI VersaProbe II X-ray Photoelectron Spectrometer. The samples were transferred to XPS with minimum exposure to the air. The binding energies were calibrated by F 1s peak of LiF at 685.0 eV.

Supporting Information

Supporting Information is available from the Wiley Online Library or from the author.

Acknowledgements
The authors acknowledge funding from MIT Lincoln Laboratory in support of this research. This work made use of the MRSEC Shared Experimental Facilities at MIT, supported by the National Science Foundation under award number DMR-14-19807. We also wish to thank Eric Morgan at Lincoln Laboratory for helpful discussions.

Received: ((will be filled in by the editorial staff))
Revised: ((will be filled in by the editorial staff))
Published online: ((will be filled in by the editorial staff))

References

[1] a) J. Cabana, L. Monconduit, D. Larcher, M. R. Palacin, *Adv. Mater.* **2010**, 22, E170; b) J. Kim, H. Kim, K. Kang, *Adv. Energy Mater.* **2018**, 1702646.

[2] a) D. Aurbach, B. D. McCloskey, L. F. Nazar, P. G. Bruce, *Nat. Energy* **2016**, 1; b) J. Lu, L. Li, J. B. Park, Y. K. Sun, F. Wu, K. Amine, *Chem. Rev.* **2014**, 114, 5611.

[3] X. Gao, Y. Chen, L. Johnson, P. G. Bruce, *Nat. Mater.* **2016**, 15, 882.

[4] a) L. Ma, T. Yu, E. Tzoganakis, K. Amine, T. Wu, Z. Chen, J. Lu, *Adv. Energy Mater.* **2018**, 8, 1800348; b) Y. C. Lu, B. M. Gallant, D. G. Kwabi, J. R. Harding, R. R. Mitchell, M. S. Whittingham, Y. Shao-Horn, *Energy Environ. Sci.* **2013**, 6.

[5] a) P. Hartmann, C. L. Bender, M. Vračar, A. K. Dürr, A. Garsuch, J. Janek, P. Adelhelm, *Nat. Mater.* **2013**, 12, 228; b) P. Adelhelm, P. Hartmann, C. L. Bender, M. Busche, C. Eufinger, J. Janek, *Beilstein J. Nanotechnol.* **2015**, 6, 1016.

[6] X. Ren, Y. Wu, *J. Am. Chem. Soc.* **2013**, 135, 2923.

[7] a) I. Landa-Medrano, R. Pinedo, X. Bi, I. Ruiz de Larramendi, L. Lezama, J. Janek, K. Amine, J. Lu, T. Rojo, *ACS Appl. Mater. Interfaces* **2016**, 8, 20120; b) B. D. McCloskey, J. M. Garcia, A. C. Luntz, *J. Phys. Chem. Lett.* **2014**, 5, 1230; c) N. Xiao, X. Ren, W. D. McCulloch, G. Gourdin, Y. Wu, *Acc. Chem. Res.* **2018**, 51, 2335.

[8] H. D. Lim, H. Park, H. Kim, J. Kim, B. Lee, Y. Bae, H. Gwon, K. Kang, *Angew. Chem., Int. Ed.* **2015**, 54, 9663.

[9] a) X. Li, S. Yang, N. Feng, P. He, H. Zhou, *Chin. J. Catal.* **2016**, 37, 1016; b) Y. Qiao, J. Yi, S. Wu, Y. Liu, S. Yang, P. He, H. Zhou, *Joule* **2017**, 1, 359; c) S. Xu, S. K. Das, L. A. Archer, *RSC Adv.* **2013**, 3, 6656; d) A. Khurram, M. He, B. M. Gallant, *Joule* **2018**, 2, 2649.

[10] a) Y. Li, A. Khurram, B. M. Gallant, *J. Phys. Chem. C* **2018**, 122, 7128; b) M. He, Y. Li, R. Guo, B. M. Gallant, *J. Phys. Chem. Lett.* **2018**, 9, 4700.

[11] K. Seppelt, *Chem. Rev.* **2015**, 115, 1296.

[12] a) X. Ren, K. C. Lau, M. Yu, X. Bi, E. Kreidler, L. A. Curtiss, Y. Wu, *ACS Appl. Mater. Interfaces* **2014**, 6, 19299; b) C. L. Bender, P. Hartmann, M. Vračar, P. Adelhelm, J. Janek, *Adv. Energy Mater.* **2014**, 4, 1301863; c) B. D. McCloskey, R. Scheffler, A. Speidel, G. Girishkumar, A. C. Luntz, *J. Phys. Chem. C* **2012**, 116, 23897.

[13] C. Xia, C. Y. Kwok, L. F. Nazar, *Science* **2018**, 361, 777.

[14] Y. C. Lu, D. G. Kwabi, K. P. C. Yao, J. R. Harding, J. Zhou, L. Zuin, Y. Shao-Horn, *Energy Environ. Sci.* **2011**, 4, 2999.

[15] a) V. Viswanathan, K. S. Thygesen, J. Hummelshøj, J. K. Nørskov, G. Girishkumar, B. D. McCloskey, A. C. Luntz, *J. Chem. Phys.* **2011**, 135, 214704; b) Z. Lyu, Y. Zhou, W. Dai, X. Cui, M. Lai, L. Wang, F. Huo, W. Huang, Z. Hu, W. Chen, *Chem. Soc. Rev.* **2017**, 46, 6046.

[16] L. Johnson, C. Li, Z. Liu, Y. Chen, S. A. Freunberger, P. C. Ashok, B. B. Praveen, K. Dholakia, J. M. Tarascon, P. G. Bruce, *Nat. Chem.* **2014**, 6, 1091.

[17] N. B. Aetukuri, B. D. McCloskey, J. M. Garcia, L. E. Krupp, V. Viswanathan, A. C. Luntz, *Nat. Chem.* **2015**, 7, 50.

[18] a) H. D. Lim, B. Lee, Y. Zheng, J. Hong, J. Kim, H. Gwon, Y. Ko, M. Lee, K. Cho, K. Kang, *Nat. Energy* **2016**, 1, 16066; b) J. B. Park, S. H. Lee, H. G. Jung, D. Aurbach, Y. K. Sun, *Adv. Mater.* **2018**, 30, 1704162.

[19] W. Yu, H. Wang, J. Hu, W. Yang, L. Qin, R. Liu, B. Li, D. Zhai, F. Kang, *ACS Appl. Mater. Interfaces* **2018**, 10, 7989.

[20] Z. Liu, L. Ma, L. Guo, Z. Peng, *J. Phys. Chem. Lett.* **2018**, 9, 5915.

[21] a) N. Watanabe, R. Hagiwara, T. Nakajima, H. Touhara, K. Ueno, *Electrochim. Acta* **1982**, 27, 1615; b) C. Pang, F. Ding, W. Sun, J. Liu, M. Hao, Y. Wang, X. Liu, Q. Xu, *Electrochim. Acta* **2015**, 174, 230.

[22] X. Cui, J. Chen, T. Wang, W. Chen, *Sci. Rep.* **2014**, 4, 5310.

[23] Z. Peng, S. A. Freunberger, Y. Chen, P. G. Bruce, *Science* **2012**, 337, 563.

[24] Y. C. Lu, H. A. Gasteiger, Y. Shao-Horn, *Electrochem. Solid-State Lett.* **2011**, 14, A70.

[25] a) J. Gao, M. A. Lowe, Y. Kiya, H. D. Abruña, *J. Phys. Chem. C* **2011**, 115, 25132; b) T. Yim, M. S. Park, J. S. Yu, K. J. Kim, K. Y. Im, J. H. Kim, G. Jeong, Y. N. Jo, S. G. Woo, K. S. Kang, *Electrochim. Acta* **2013**, 107, 454.

[26] C. B. Stubblefield, R. O. Bach, *J. Chem. Eng. Data* **1972**, 17, 491.

[27] D. A. Wynn, M. M. Roth, B. D. Pollard, *Talanta* **1984**, 31, 1036.

[28] N. Xin, Y. Sun, M. He, C. J. Radke, J. M. Prausnitz, *Fluid Phase Equilib.* **2018**, 461, 1.

[29] L. Zámostná, T. Braun, *Angew. Chem.* **2015**, 127, 10798.

[30] a) U. Mayer, V. Gutmann, W. Gerger, *Monatshefte für Chemie/Chemical Monthly* **1975**, 106, 1235; b) V. Gutmann, *Electrochim. Acta* **1976**, 21, 661.

[31] a) L. Johnson, C. Li, Z. Liu, Y. Chen, S. A. Freunberger, P. C. Ashok, B. B. Praveen, K. Dholakia, J. M. Tarascon, P. G. Bruce, *Nat. Chem.* **2014**, 6, 1091; b) K. M. Abraham, *J.*

Electrochem. Soc. **2015**, 162, A3021; c) D. Xu, Z. L. Wang, J. J. Xu, L. L. Zhang, X. B. Zhang, *Chem. Commun.* **2012**, 48, 6948.

[32] R. D. Rauh, F. S. Shuker, J. M. Marston, S. B. Brummer, *J. Inorg. Nucl. Chem.* **1977**, 39, 1761.

[33] S. Lau, L. A. Archer, *Nano Lett.* **2015**, 15, 5995.

[34] B. Liu, W. Xu, J. Zheng, P. Yan, E. D. Walter, N. Isern, M. E. Bowden, M. H. Engelhard, S. T. Kim, J. Read, *ACS Energy Lett.* **2017**, 2, 2525.

[35] a) G. Erker, *Dalton Trans.* **2005**, 11, 1883; b) S. Döring, G. Erker, R. Fröhlich, O. Meyer, K. Bergander, *Organometallics* **1998**, 17, 2183.

[36] a) L. F. Li, H. S. Lee, H. Li, X. Q. Yang, K. W. Nam, W. S. Yoon, J. McBreen, X. J. Huang, *J. Power Sources* **2008**, 184, 517; b) X. Sun, H. S. Lee, X. Q. Yang, J. McBreen, *Electrochem. Solid-State Lett.* **2001**, 4, A184.

[37] a) Z. Chen, K. Amine, *J. Electrochem. Soc.* **2006**, 153, A1221; b) X. Sun, H. S. Lee, X. Q. Yang, J. McBreen, *Electrochem. Solid-State Lett.* **2002**, 5, A248.

[38] G. B. Han, J. N. Lee, J. W. Choi, J. K. Park, *Electrochim. Acta* **2011**, 56, 8997.

[39] M. Herstedt, M. Stjerndahl, T. Gustafsson, K. Edström, *Electrochem. Commun.* **2003**, 5, 467.

[40] a) D. Zheng, Q. Wang, H. S. Lee, X. Q. Yang, D. Qu, *Chemistry* **2013**, 19, 8679; b) Q. Wang, D. Zheng, M. E. McKinnon, X. Q. Yang, D. Qu, *J. Power Sources* **2015**, 274, 1005.

[41] V. P. Reddy, M. Blanco, R. Bugga, *J. Power Sources* **2014**, 247, 813.

[42] X. Y. Yang, J. J. Xu, D. Bao, Z. W. Chang, D. P. Liu, Y. Zhang, X. B. Zhang, *Adv. Mater.* **2017**, 29, 1700378.

Significant improvement of rate capability of Li-SF_6 cells is achieved by controlling the formation of LiF. Two viable strategies, moderately elevating temperature to 50 °C or using an anion receptor (TPFPB) as additive in electrolyte, can increase attainable capacity by a factor of 10 or 25, respectively, at high current density (120 μA cm^{-2}).

Keyword: Batteries

H. Gao, Y. Li, R. Guo and Prof. B. M. Gallant*

Controlling Fluoride-Forming Reactions for Improved Rate Capability in Lithium-Gas Conversion Batteries

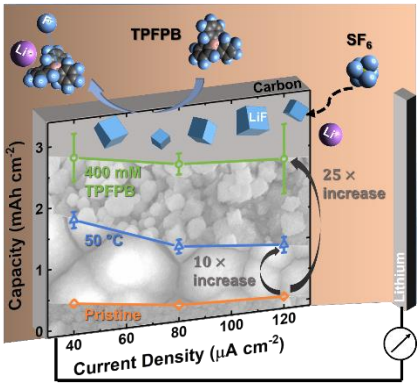

Supporting Information

Controlling Fluoride-Forming Reactions for Improved Rate Capability in Lithium-Gas Conversion Batteries

*Haining Gao, Yuanda Li, Rui Guo, and Betar M. Gallant**

Additional Experimental Methods

Electrochemical impedance spectroscopy (EIS): EIS analysis was conducted on two-electrode Swagelok cells. A potential perturbation of 5 mV was applied in a frequency range from 1 MHz to 100 mHz at open circuit voltage.

Quantifcation of LiF yield: The amount of LiF generated after discharge was determined using the following procedure: the cathode and separator of the discharged cell were extracted and soaked in 3 mL D_2O overnight to dissolve solid LiF. A portion of this solution was transferred into a capped NMR tube with 136 mM 2,2,2-trifluoroethanol (TFE) added as an internal reference. The concentration of LiF was obtained by comparing the integrated peak area of TFE and LiF in the ^{19}F NMR spectrum. Additional information can be found in our previous publication.[1]

Calculation of TPFPB-induced theoretical capacity gain:

Total mole of TPFPB (n_{TPFPB}) in a volume V [L] of electrolyte ($V = 150 \times 10^{-6}$ L) at a concentration of c [M]: $n_{\mathrm{TPFPB}} = c \times V$

Total mole of LiF (n_{LiF}) dissolved by TPFPB (assuming each TPFPB molecule dissolves only one molecule of LiF): $n_{\mathrm{LiF}} = n_{\mathrm{TPFPB}}$

The solubilization of each LiF molecule corresponds to one electron transferred during discharge, so the total additional charge transfer (Q, [C]) corresponding to n_{LiF} mol of LiF: $Q = F \times n_{\mathrm{LiF}}$ (F denotes Faraday constant, 96485 C mol^{-1}).

Thus the theoretical capacity gain is: $Q = F \times c \times V \div 3.6$ [C/mAh]

For example, at concentration of c = 0.05 M, $Q = \left(96485 \frac{C}{mol}\right) \times (0.05\,M) \times (150 \times 10^{-6}\ \mathrm{L}) \div 3.6\ (\mathrm{C/mAh}) = 0.20\ (\mathrm{mAh})$.

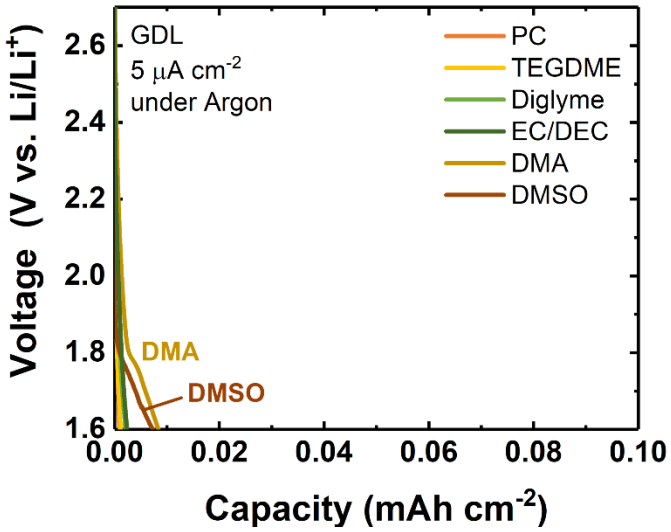

Figure S1. Galvanostatic discharge of Li/Gas Diffusion Layer (Li/GDL) cells in different electrolyte solvents (PC, EC/DEC, TEGDME, diglyme, DMA and DMSO) under an argon headspace at a current density of 5 μA cm^{-2}. The electrolyte was 0.1 M $LiClO_4$ (with the exception of 0.07 M in diglyme) and the cutoff voltage was 1.6 V vs. Li/Li^+.

Table S1. Donor Number (DN), acceptor number (AN) and reported LiF solubility (at room temperature, unless otherwise indicated) of different solvents.

Solvent	DN[2]	AN[2a, 3]	LiF solubility(g L^{-1})
PC	15.1	18.3	0.13[4]
EC	16.4	22.2	5.52[4] (40 °C)
DEC	16	6.2	<0.01[5]
Diglyme	18[6]	9.9	
TEGDME	16.6	10.5[7]	
DMA	27.8	13.6	
DMSO	29.8	19.3	0.37[8]

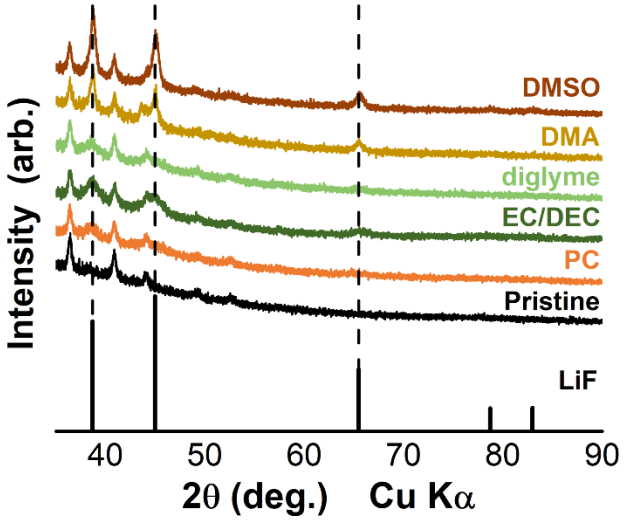

Figure S2. X-ray diffraction (XRD) patterns of fully discharged Vulcan Carbon (VC) cathodes in different electrolyte solvents containing 0.1 M $LiClO_4$ (with the exception of 0.07 M in diglyme) at a current density of 75 mA g_C^{-1}. The cutoff voltage was 1.6 V vs. Li/Li^+, (capacity = 3975, 2860, 1430, 1065, and 800 mAh g_C^{-1} for cells discharged with DMSO, DMA, diglyme, EC/DEC, and PC electrolyte respectively).

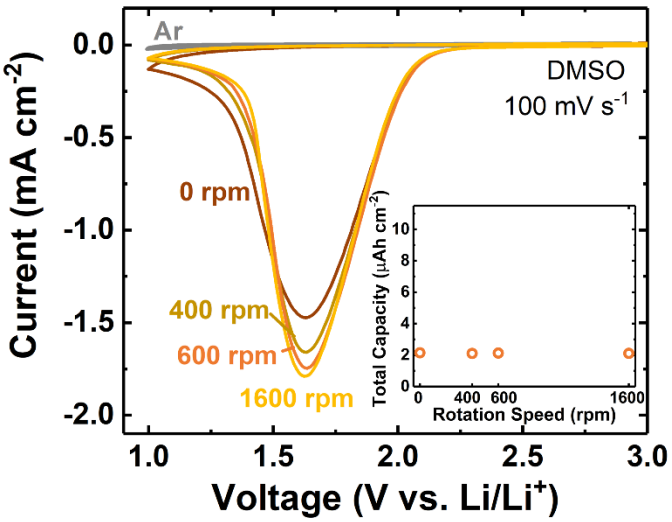

Figure S3. Rotating disk electrode (RDE) measurement of Li-SF_6 cells with DMSO electrolyte. The total integrated capacity of the 1st reduction cycle at various rotation speeds (0, 400, 600, 1600 rpm) is shown in the inset. The scan rate is 100 mV s^{-1}, with a lower cutoff voltage of 1 V vs. Li/Li^+. For all rotation rates investigated, negligible current can be detected after the 1st cycle in DMSO electrolyte. The argon background (at 1600 rpm, which was representative of all argon scans over different rotation rates) is shown in gray.

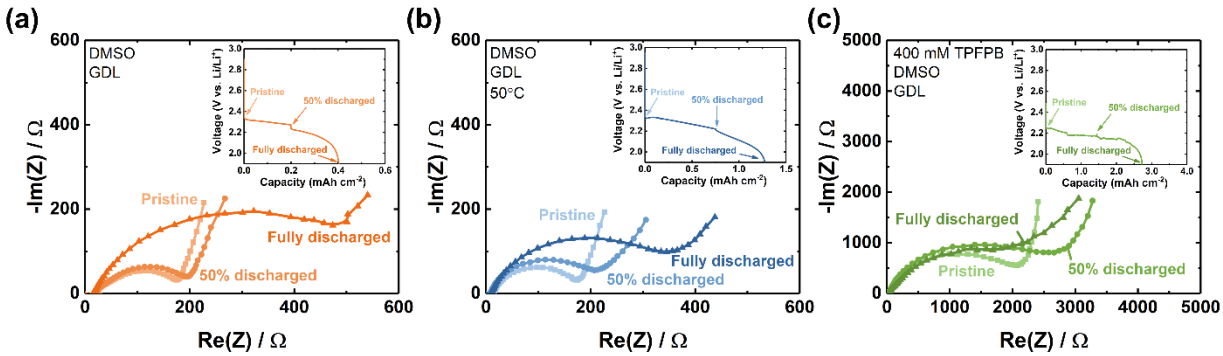

Figure S4. Nyquist plots of Li-SF_6 cells with 0.1 M $LiClO_4$/DMSO electrolyte at different depths of discharge at **(a)** room temperature (RT), **(b)** 50 °C, and **(c)** with 400 mM TPFPB additive at RT. The corresponding discharge states at which impedances were measured are indicated in the inset.

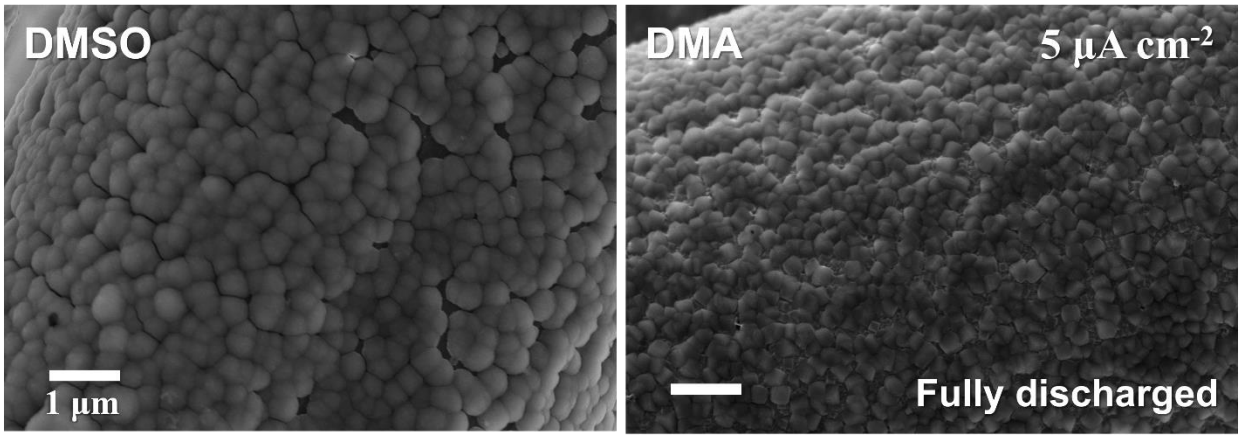

Figure S5. Scanning electron microscopy (SEM) images of gas diffusion layer (GDL) cathodes in Li-SF_6 cells after full galvanostatic discharge in DMSO or DMA electrolyte (as indicated). The current density in both cases was 5 µA cm^{-2} (capacity = 1.3 and 0.6 mAh cm^{-2} for cells discharged with DMSO and DMA, respectively). Scale bar = 1 µm in both images.

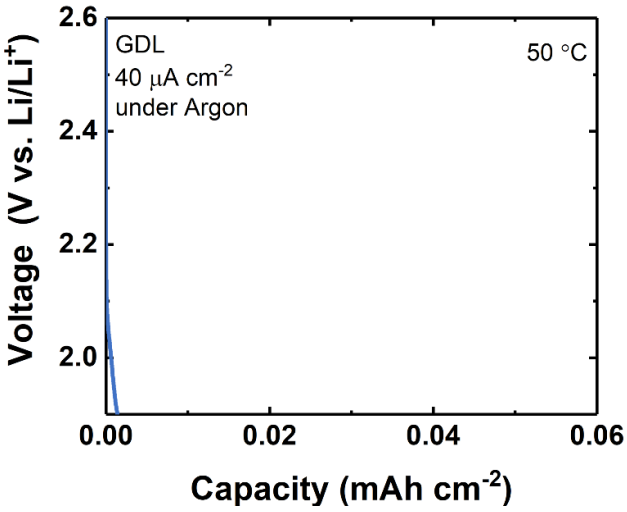

Figure S6. Galvanostatic discharge of Li/GDL cells at 50 °C in 0.1 M $LiClO_4$/DMSO electrolyte under an argon headspace and a current density of 40 μA cm^{-2}, with a cutoff voltage of 1.9 V vs. Li/Li^+.

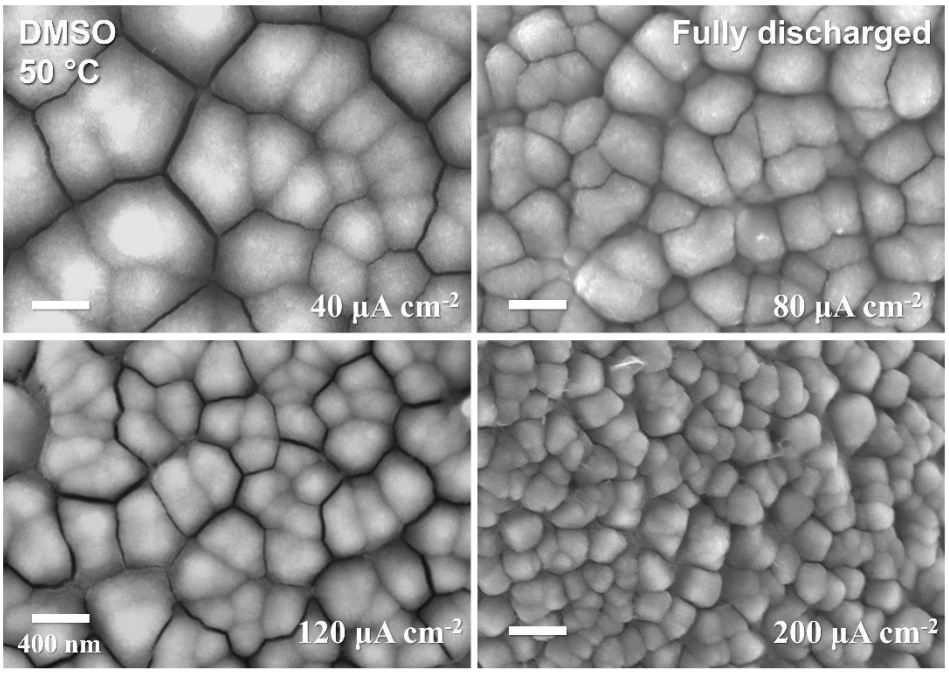

Figure S7. Scanning electron microscopy (SEM) images of gas diffusion layer (GDL) cathodes in Li-SF_6 cells fully discharged in DMSO electrolyte at 50 °C at current densities of 40, 80, 120 and 200 μA cm^{-2} (capacity = 1.8, 1.0, 1.0, and 0.9 mAh cm^{-2} respectively). The scale bar = 400 nm in all images.

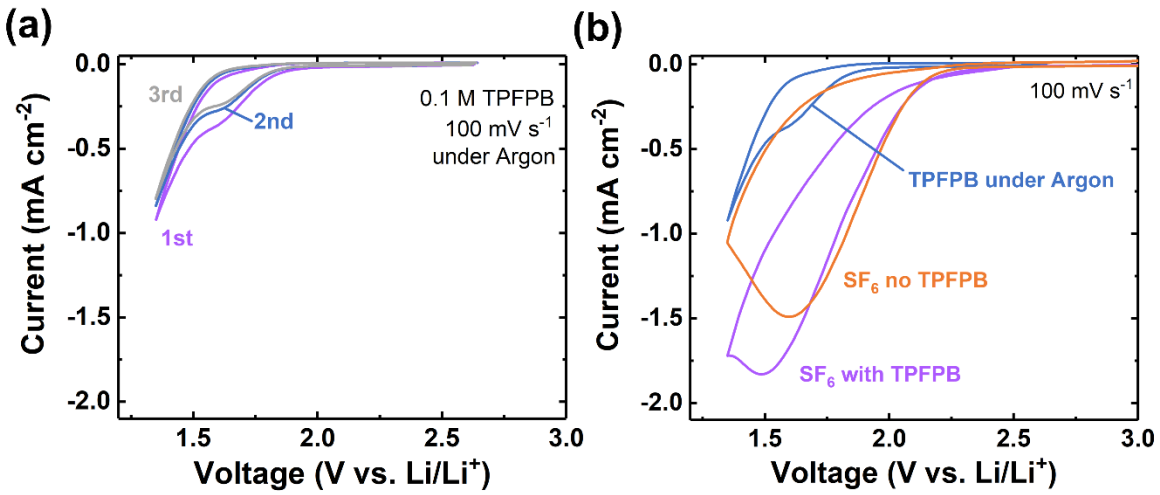

Figure S8. **(a)** Cyclic voltammetry of 0.1 M $LiClO_4$/DMSO electrolyte containing 0.1 M TPFPB under an argon headspace at a scan rate of 100 mV s^{-1}. **(b)** Comparison of 1st scan in Figure S8a (as background measurement: TPFPB under Argon), Figure 5b (SF_6 in DMSO electrolyte without TPFPB), and Figure 5c (SF_6 in DMSO electrolyte with 0.1 M TPFPB).

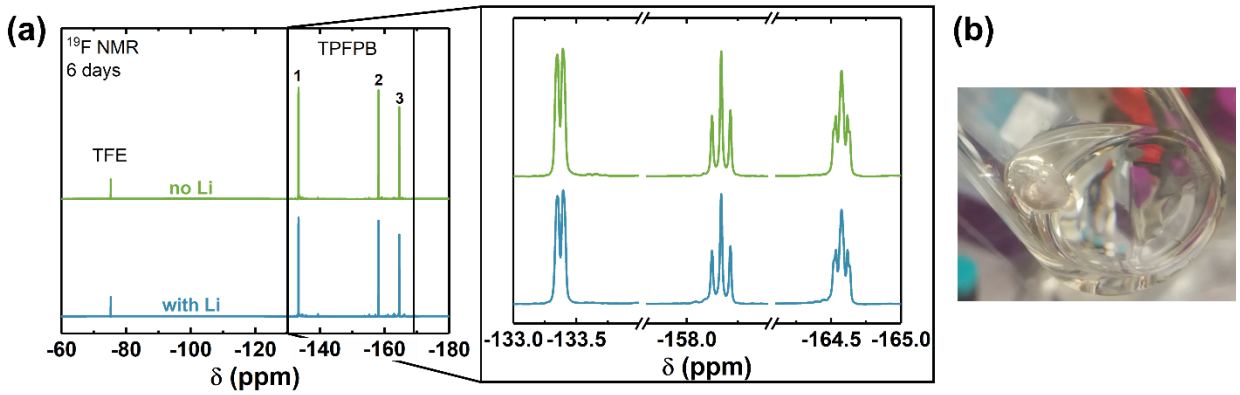

Figure S9. **(a)** ^{19}F NMR of 400 mM TPFPB in 0.1M $LiClO_4$/DMSO electrolyte with/without PC-stabilized Li soaked for six days. To avoid possible reaction between TPFPB and the reference (2,2,2-Trifluoroethanol, TFE), the measurements were conducted using coaxial NMR tubes. The inner tube was filled with 136 mM TFE in DMSO-d_6 with the outer tube containing the electrolyte. **(b)** Photograph of PC-stabilizd Li after soaked in DMSO electrolyte containing 400 mM TPFPB for six days, showing negligible reactivity.

Table S2. Calculation of TPFPB concentration from NMR result in Figure S9, from a nominal added concentration of 400 mM. (Integrals were normalized to that of reference peak. The volume ratio between outer and inner tube is 5.82.)* The case with 'No Li' is included to show the typical measurement error occurring without TPFPB present.

	Integral				**TPFPB concentration**
	Peak 1	Peak 2	Peak 3	Total	**(mM)**
No Li	35.13	15.40	32.72	83.25	389
With Li	35.59	15.96	33.33	84.88	396

* The volume ratio was calibrated by using two different references with known concentration: 136 mM TFE and 129 mM trifluoroacetic acid (TFA) in DMSO-d_6, in inner and outer tubes respectively.

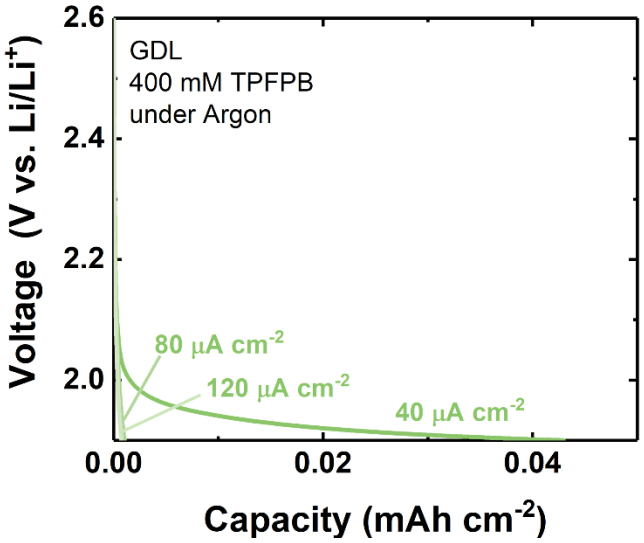

Figure S10. Galvanostatic discharge of Li/GDL cells in 0.1 M $LiClO_4$/DMSO electrolyte containing 0.4 M TPFPB under an argon headspace. The cutoff voltage was 1.9 V vs. Li/Li^+.

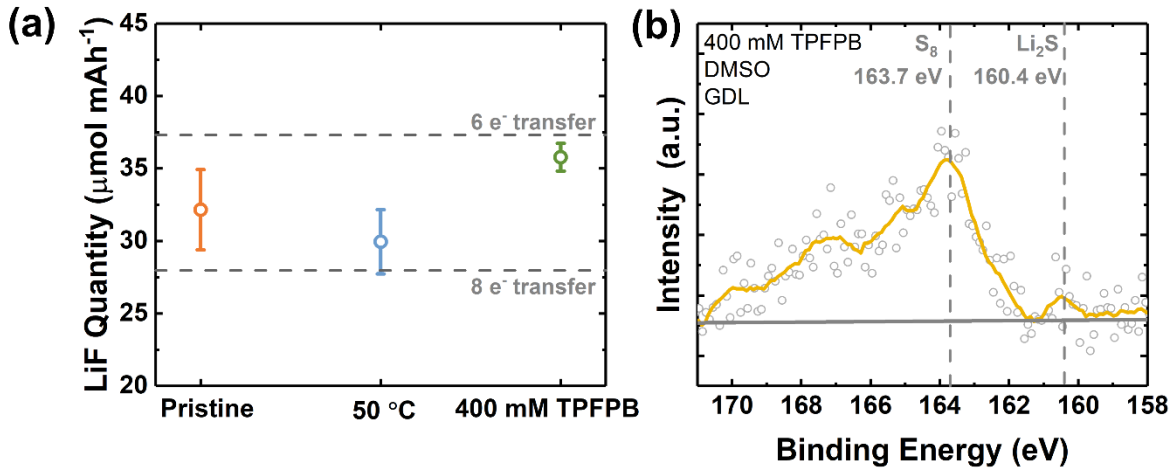

Figure S11. **(a)** Quantification of LiF formed after galvanostatic discharge at 50 °C and RT with or without TPFPB additive, in 0.1 M $LiClO_4$/DMSO electrolyte at 40 μA cm^{-2}. Dashed lines indicate theoretical values of LiF formed per mAh of discharge capacity, which correspond to 28.0 and 37.3 μmol mAh^{-1} for 8 e^- transfer ($Li + SF_6 = Li_2S + LiF$) and 6 e^- transfer ($Li + SF_6 = S + LiF$) assumptions respectively. The averages and error bars represent statistics from more than three samples for each condition. **(b)** S 2p high-resolution XPS spectra of a fully discharged cathode (capacity = 3.0 mAh cm^{-2}) at 40 μA cm^{-2} in 0.1 M $LiClO_4$/DMSO electrolyte with 400 mM TPFPB.

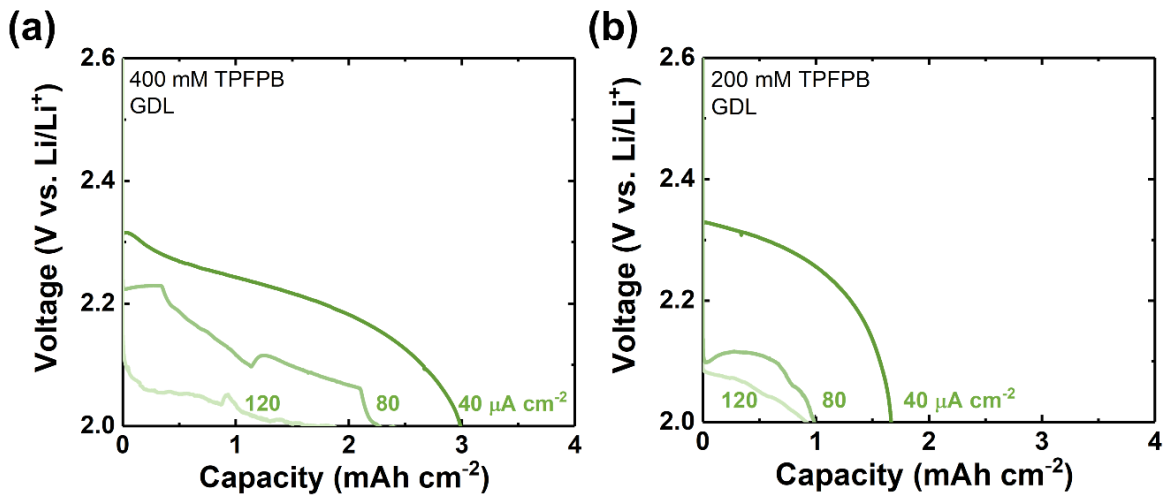

Figure S12. Rate capability of Li-SF_6 cells with **(a)** 400 mM and **(b)** 200 mM of the TPFPB additive in 0.1 M $LiClO_4$/DMSO electrolyte. Galvanostatic discharge was conducted at a current density of 40, 80, or 120 μA cm^{-2} with GDL electrodes and a cutoff voltage of 2.0 V vs. Li/Li^+. The relatively large noise in the voltage profiles is caused by room temperature variation during discharge, as TPFPB was found to increase the thermal sensitivity of cells. We verified that all cells made at the same time showed exactly the same trend in voltage fluctuation, and that the noise could be eliminated if the test were performed in a constant temperature incubator.

References

[1] Y. Li, A. Khurram, B. M. Gallant, *J. Phys. Chem. C* **2018**, 122, 7128

[2] a) U. Mayer, V. Gutmann, W. Gerger, *Monatshefte für Chemie/Chemical Monthly* **1975**, 106, 1235; b) V. Gutmann, *Electrochim. Acta* **1976**, 21, 661.

[3] P. J. Michelsen, *Degree Thesis*, Rochester Institute of Technology, 12, **1990**.

[4] J. Jones, M. Anouti, M. Caillon-Caravanier, P. Willmann, D. Lemordant, *Fluid Phase Equilib.* **2009**, 285, 62.

[5] J. Jones, M. Anouti, M. Caillon-Caravanier, P. Willmann, P.-Y. Sizaret, D. Lemordant, *Fluid Phase Equilib.* **2011**, 305, 121.

[6] L. Lutz, W. Yin, A. Grimaud, D. Alves Dalla Corte, M. Tang, L. Johnson, E. Azaceta, V. Sarou-Kanian, A. Naylor, S. Hamad, *J. Phys. Chem. C* **2016**, 120, 20068.

[7] K. Abraham, *ECS Trans.* **2012**, 41, 27.

[8] N. Xin, Y. Sun, M. He, C. J. Radke, J. M. Prausnitz, *Fluid Phase Equilib.* **2018**, 461, 1.